ACS Sustainable Chemistry & Engineering

pubs.acs.org/journal/ascecg

Research Article

Converting Pomelo Peel into Eco-friendly and Low-Consumption Photothermic Biomass Sponge toward Multifunctioal Solar-to-Heat Conversion

Chang Zhang, Peng Xiao,* Feng Ni, Luke Yan, Qingquan Liu, Dong Zhang, Jincui Gu, Wenqin Wang,* and Tao Chen*

Cite This: *ACS Sustainable Chem. Eng.* 2020, 8, 5328−5337

Read Online

ACCESS | Metrics & More | Article Recommendations | Supporting Information

ABSTRACT: Converting waste into versatile materials has been considered as an effective strategy to tackle environmental issues such as shortages in food, clean water, and energy. Conventional carbonization technology has provided an effective approach for constructing photothermal materials for interfacial evaporation or crude oil removal. However, high energy consumption, poor shape retention, and weak mechanical strength have significantly hindered the practical application of conventional carbonization technology. This work discusses how a biomass-derived sponge from discarded pomelo peel (PP) may be used to collect photothermal polypyrrole in a cost-effective way with mild reaction. The photothermic sponge which is derived from this process, can then be effectively employed to realize solar enhanced water evaporation and heavy crude oil removal. The polypyrrole-functionalized pomelo peel (FPyPP) can be attained by a mild, one-pot wet oxypolymerization method, resulting in over 95% absorption of sunlight and evaporation rates of about 1.22 kg/m^2 under the sun. Furthermore, the concentrated heat on the sponge surface can efficiently reduce the viscosity of heavy crude oil and thereby lead to an effective cleanup. This study aims to provide a low-cost, low-energy-consumption, and eco-friendly approach to the acquisition of the multifunctional photothermic sponge by recycling the waste and demonstrating potential applications in tackling clean water generation and polluted water treatment.

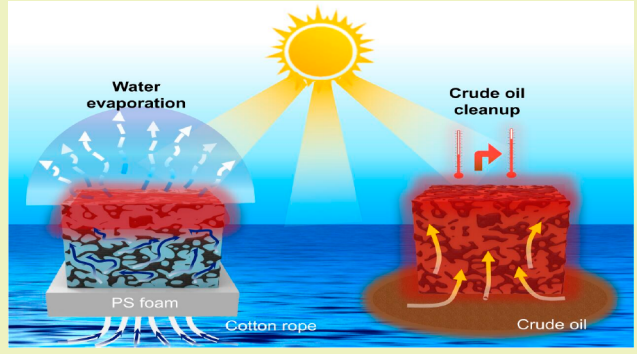

KEYWORDS: *Polypyrrole, Biomass sponge, Low-energy-consumption, Photothermic conversion, Water treatment*

INTRODUCTION

With a rapidly increasing population, environmental pollution, and energy and water scarcity, the world is currently going through a rather challenging period.[1,2] In particular, the unreasonable handling of abundant food waste may cause adverse environmental and social effects, such as the decline of available land, adverse global climate change, and economic consumption. As such, the means of effectively converting otherwise wasted resources into valuable and functional materials toward sustainable applications in a mild, low-energy-consumption, and eco-friendly way has become an issue of significant importance.[3−6] There are also alternative opportunities to alleviate the social and environmental issues. Solar energy, as a renewable and sustainable resource, has been extensively exploited to realize diverse solar-to-thermal conversion applications,[7−11] including photothermic interfacial water evaporation,[12−15] thermoelectric converters,[16−18] thermal management devices,[19−21] mechanical actuators,[22,23] and solar heated oil absorbers.[24,25] In recent years, extensive efforts have been dedicated to develop a variety of chemically synthesized solar absorbers, such as noble metal particles,[26−28] carbon nanostructures,[29−33] functionalized hydrogels,[34−37] and sponges.[38−41]

Specifically, to alleviate the adverse effects of secondary pollution on the environment, naturally occurring and abundantly available trees,[42] mushrooms,[43] and even lotus seedpods[44] have been carbonized at high temperatures to fabricate photothermal materials.[45,46] Note that the naturally occurring raw materials have provided a very useful pathway to decrease the usage of fully synthesized materials; this, in turn, can significantly reduce the environmental pollution as opposed to the conventional carbonization processes which may result in poor shape retention, low mechanical strength,

Received: January 26, 2020
Revised: March 5, 2020
Published: March 23, 2020

https://dx.doi.org/10.1021/acssuschemeng.0c00681
ACS Sustainable Chem. Eng. 2020, 8, 5328−5337

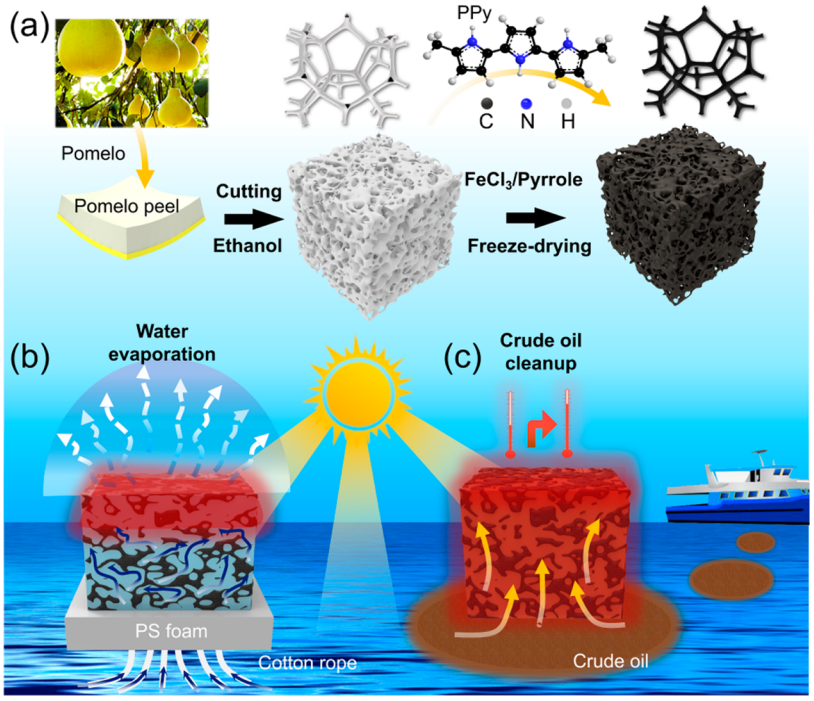

Figure 1. (a) Schematic illustration of the fabrication of polypyrrole-functionalized pomelo peel for a photothermal solar absorber. (b) Resulted FPyPP employed to realize solar-driven interfacial water evaporation. (c) Crude oil removal.

and rigorous fabrication conditions. In addition, given the economic and environmental factors, the energy-intensive carbonization technology and relatively expensive raw materials have severely hindered progress toward further sustainable and low-consumption development. Therefore, it is highly desirable to develop photothermic materials to operate in a mild, low-cost, eco-friendly, and sustainable way.

As a typical food byproduct which is usually discarded, pomelo peel (PP) has a naturally occurring interconnected porous structure that can act as an excellent option for a sponge-like template. However, other fruit or vegetable waste peels with relatively thin inner peels that are not suitable for *in situ* chemical modification have alternatively been carbonized into powders and further fabricated into films for photothermic applications. As such, it is expected to be an alternative for a biocompatible and low-cost three-dimensional (3D) porous water transportation substrate. Nevertheless, high sunlight reflection and low absorption of the peels severely hinder the solar-to-thermal conversion. As a typical conjugated and conducting polymer, polypyrrole (PPy) is endowed with good biocompatible and photothermal properties, which have been extensively explored to conduct solar steam generation and solar-assisted heating and actuating.[47−49] In addition, PPy can be *in situ* synthesized via a wet method in a facile and accessible way. Thus, PPy is expected to be a competitive alternative to functionalize porous PP for improved photothermal materials. In this work, we have developed a multifunctional photothermic sponge composed of conjugated PPy polymers and self-templated PP waste in a mild, low-energy-consumption, and eco-friendly way. The PP waste can be sustainably recycled and effectively converted into a photothermic sponge *via* a wet method of *in situ* PPy decoration. The photothermal sponge can be integrated into a bilayer evaporator to realize effective interfacial solar-driven water evaporation. Furthermore, it can be further applied to the surface of heavy crude oil in order to achieve solar-heating oil removal. The biomass-derived sponge with biocompatible PPy functionalization is expected to provide an environmentally friendly platform to tackle water shortages and emergency oil pollution, thereby reducing secondary pollution or potential negative effects on the environments.

MATERIALS AND METHODS

Fabrication of the FPyPP. First of all, the fresh pomelo peel (PP) was obtained by taking the shells from the pomelos purchased from local markets. Note that the yellow epidermis of PP needs to be removed because of its dense and nonporous structure, and only about 1 cm of white inner part is left for our systems. The samples of PP were cut into pieces and dehydrated in ethanol solution for 1 day; at the same time ethanol also could widely open the internal pores of PP by removing the bio-oil. Subsequently, the resulted PP was soaked in $FeCl_3$ solution (0.5 mol/L) for 1 h, and then was immersed into 0.2 mol/L CH_3Cl solution of pyrrole for 3 h to acquire the polypyrrole-functionalized PP (PyPP). To remove the residual and physically absorbed oxidizing agent of $FeCl_3$, the achieved PyPP was thoroughly rinsed using the deionized water for several times until all of the free ions such as Fe^{3+}, Fe^{2+}, and Cl^- were removed from its surface. Prior to final freeze-drying procedure, the resulted PyPP samples were immersed in water in a confined vessel for further pH measurement, in which procedure the pH was rigorously controlled in the range of 6 and 8. Finally, freeze-dried PyPP (FPyPP) was obtained by putting PyPP in a freeze-dryer for 24 h.

Saturated Water Absorption Experiments. First, three samples (FPP, FPyPP, and fresh PP) were cut into the same shape, weighed, and subsequently immersed in the water, respectively. After 10 min, the resulted samples were weighed again on an electronic balance. The whole process was repeated for three times to calculate the average mass of water absorption.

Preparation of a Solar-Driven Evaporation Device. Quartz beakers (10 mL) were chosen as the containers for a solar-driven evaporation device. The commercial cotton fibers and polystyrene (PS) foam were used as a water pumping path and thermal insulating layer, respectively. FPyPP was cut into a pie shape (diameter = 2.5

https://dx.doi.org/10.1021/acssuschemeng.0c00681
ACS Sustainable Chem. Eng. 2020, 8, 5328−5337

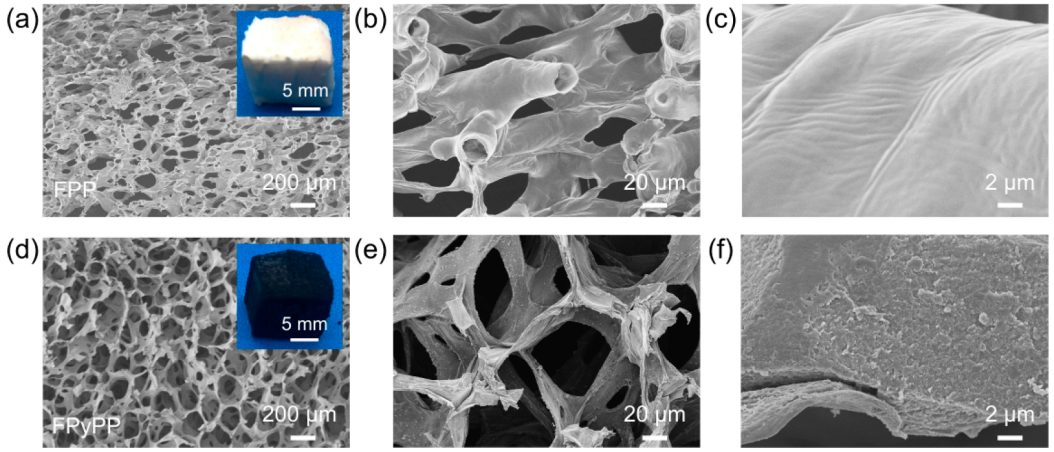

Figure 2. (a–c) SEM images of freeze-dried PP (FPP), demonstrating porous structures and smooth surface morphology. Inset of panel a: digital photograph of FPP. (d–f) SEM images of the porous structures of FPyPP with rough surface. Inset of panel d: digital photograph of FPyPP.

cm, thickness = 1 cm) and put onto the PS foam. Its bottom was completely attached to cotton fibers.

Solar-Driven Photothermal Water Purification Experiment. The resulted solar-driven purification devices were set under the irradiation of a Solar Simulator (HM-Xe500W) equipped with an AM 1.5 G filter for water purification. The mass change (m) of water during evaporation was recorded using an electronic balance.

Cr(VI) Removal Experiments. *Adsorption Experiment.* A 5×10^{-3} wt % amount of potassium dichromate ($K_2Cr_2O_7$) solution was adopted to simulate raw water contained Cr(VI). The FPyPP was cut into small pieces (4 g) and put into $K_2Cr_2O_7$ solution (2000 mL), and the speed of the magnetic agitator (IKA RCT basic) was 1500 rpm. Finally, various water samples could be obtained and all of the Cr(VI) removal tests were conducted at room temperature (20 °C).

Determination of Cr(VI) Solution Concentration. Chromogenic reagent (diphenylcarbazide) was dissolved in 50 mL of acetone and then diluted to 100 mL by deionized water. A 200 μL aliquot of the above solution was added to 10 mL of water samples. Afterward, 50 μL of 1 + 1 sulfuric acid solution and 50 μL of 1 + 1 phosphoric acid solution were added into water samples, which were shaken and then stood for 10 min. The Cr(VI) concentration in solution was determined by the colorimetric method. Solution absorbance was recorded via a TU-1810 UV–vis spectrophotometer (Purkinje General Instrument Co.).

Cleanup Highly Viscous Crude Oil Experiments. First, crude oil (about 50 μL) was dropped on the water surface. Subsequently, the samples were cut into $0.8 \times 0.8 \times 0.5$ cm^3 and then were put on the water for solar-driven crude oil absorption. All absorption experiments were conducted under sun irradiation with the intensity of 1 kW/m^2.

Characterization. The samples were freeze-dried at −60 °C by using a freeze-dryer (LGJ-10J). Scanning electron microscope (SEM; Hitachi-S4800, Japan) was employed to acquire the surface morphology of a series of samples. The surface temperature of the evaporators and the IR images were measured using an infrared thermal imager (TG165, FLIR, US). The chemical composition and elemental maps of samples were measured by energy dispersive X-ray spectroscopy (EDS; Thermo Scientific, USA). X-ray photoelectron spectroscopy (XPS) analysis was performed on a Shimadzu Axis Ultra DLD spectroscope, using C–O (α) as radiation resource. Raman spectra were obtained by an R-3000HR spectrometer (Raman Systems, Inc., R-3000 series) using a green LED laser (532 nm). The contact angle was carried out by a contact angle meter (DCAT21), using a 3 μL droplet as an indicator. The ion concentrations of anions in the water samples were tested by inductively coupled plasma atomic emission spectroscopy (ICP-AES; NexION 300X). The reflection and transmittance spectra were recorded using an ultraviolet–visible–near-infrared spectrophotometer equipped with an integrating sphere (Lambda 950). The thermal conductivity of materials was evaluated by Laser Thermal Instruments (LFA457).

RESULTS

The fresh PP is massively available in our daily life, which is usually considered as food waste. In our system, this food waste, as biocompatible materials, was selected to turn into a useful material again (Figure 1a). Typically, the fresh PP was obtained via removing its yellow epidermis, whose average thickness is about 1.5 mm (Figure S1). Subsequently, the fresh PP experienced a chemical modification to acquire a favorable phototo-thermal property. The fresh PP was first rinsed with ethanol to remove internal bio-oil; then the fresh PP processed was immersed into the $FeCl_3$ solution, and Fe^{3+} can be readily absorbed onto the porous structure with a yellow color. Following a pyrrole oxypolymerization process, a black-color polypyrrole-functionalized pomelo peel (PyPP) can be finally achieved (Figure S2). Due to the abundant water molecules inside the peel, the porous network may experience a prominent collapse process when exposed to the environment for a long time. After a series of rigorous rinsing and subsequent freeze-drying procedures, FPyPP can finally be obtained. This porous photothermal material can be integrated into the designed device for solar-driven interfacial water evaporation (Figure 1b). Moreover, considering the favorable solar-to-thermal conversion performance, FPyPP can also be in situ heated to absorb the heavy crude oil for unpowered emergency treatment (Figure 1c).

Moreover, the microstructures of freeze-dried pomelo peel (FPP) before and after modification were also investigated through SEM images. As shown in Figures 2a, abundant porous structure in micron-scale can be clearly observed in FPP. It is noted that these numerous pores can endow FPP with favorable capillary force for water pumping. On top of that, the surface of FPP demonstrates hollow structures and smooth morphology (Figures 2b and 2c). After introduction of conjugated PPy polymer, the color of the FPP can experience a remarkable change from white to black (inset of Figure 2d), which can effectively improve the capability of light absorption. In addition, the pore size and distribution of FPP and PPy modified FPP was also counted through abundant SEM images, resulting in the size distribution ranging from 50 to 300 μm (Figure S3a). However, compared with the FPP, it is clearly observed that the pore size can experience an increase

https://dx.doi.org/10.1021/acssuschemeng.0c00681
ACS Sustainable Chem. Eng. 2020, 8, 5328–5337

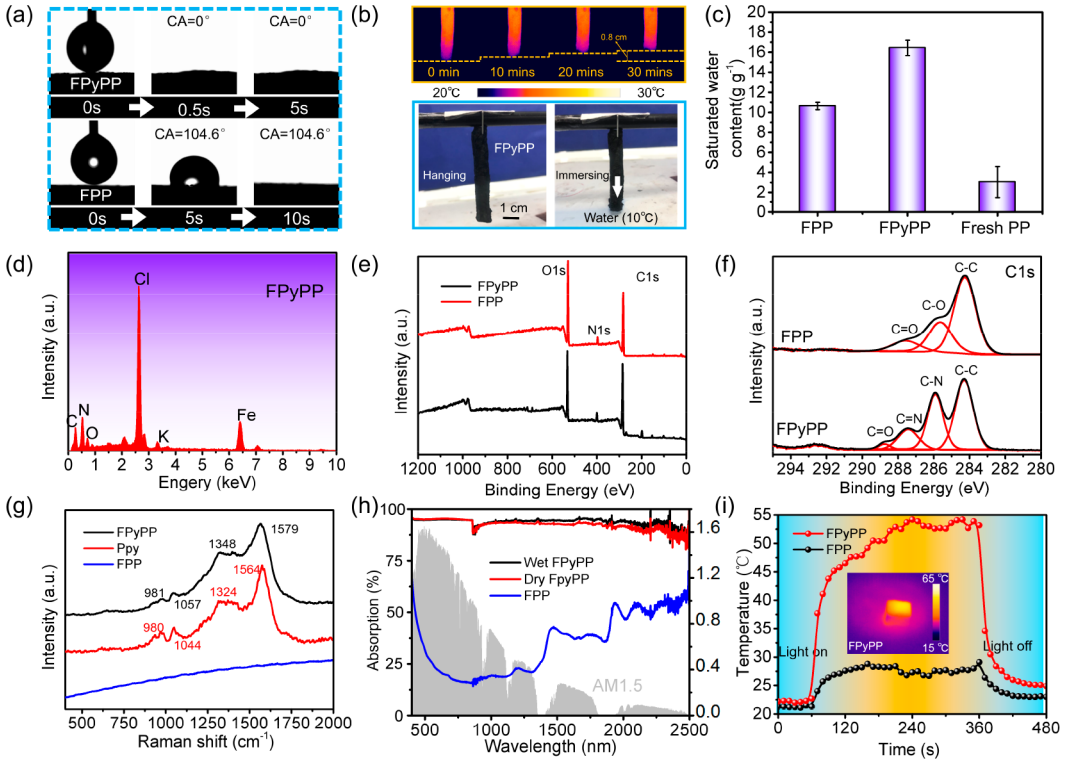

Figure 3. (a) Water contact angles of FPP and FPyPP. (b) Infrared images and photographs of FPyPP, demonstrating favorable capability of water pumping. (c) Saturated water content of fresh PP, FPP, and FPyPP. (d) EDS analysis of FPyPP. (e) XPS spectra of FPP and FPyPP. (f) High-resolution XPS spectra of FPP and FPyPP. (g) Raman spectra of FPP, FPyPP, and PPy. (h) UV−vis−IR spectra of FPP and dry and wet FPyPP. (i) Temperature versus time curves of FPP and FPyPP. Inset: Corresponding 2D IR image.

of PPy modified one (Figure S3b). This phenomenon may derive from the potential collapse of some hollow structures of FPP. It is supposed that the physical interaction between PPy and FPP may break the hollow tube inside the FPP and increase the pore sizes, which will be studied in further work.

Additionally, there are different porous structures demonstrated in different directions of FPyPP (Figure S4). To further explore the structural differentiation, SEM images of FPP were also characterized, which presented a similar structure feature. The result can further clarify that the anisotropic structure may derive from the original PP (Figure S5). Microscopically, the FPyPP represents a relatively rougher surface than that of the FPP, which is expected to remarkably enhance the light absorption (Figure 2f). Besides, we also prepared the sample of the carbonized pomelo peel (CPP) to compare its mechanical and photothermal performance with FPyPP. The CPP was obtained by heating the freeze-drying PP in a tube furnace, which was displayed in Figure S6a. Due to the porous structures and relatively weak strength of PP, the carbonized one can experience a remarkable collapse process. Microscopically, the micropores in the interior of CPP present smaller feature than that of FPyPP (Figure S6b and S6c). It is supposed that the collapsed pores may affect the performance of water pumping, which will be further studied in the photothermal and evaporation experiments. In addition, the mechanical properties of FPyPP and CPP were also investigated. As shown in Figure S7, the FPyPP demonstrates stronger mechanical strength than that of direct carbonization of pomelo peel (CPP). It can be clearly observed that compared with the favorable recovery of FPyPP, the CPP via the carbonization method is more fragile, which can be easily destroyed into powers.

Since FPP can efficiently absorb the water molecules through the capillary pores, water contact angle (WCA) measurement was conducted to investigate the water absorbing capability. As shown in Figure 3a, 3 μL of water droplet with was dropped onto the surface of FPP, resulting in complete water absorption within 10 s. After PPy modification, the water pumping performance has been apparently elevated, in which the water droplet can quickly penetrate into the FPyPP within 5 s. This phenomenon may derive from the introduction of N−H groups and Fe^{3+} doping on PPy polymer, which can effectively enhance the interaction between water molecules and modified polymers. In addition, the performance of water pumping in the vertical direction was also investigated. An FPyPP sample in stripe shape (0.8 × 0.8 × 8 cm) was employed to qualitatively characterize the climbing behavior of water molecules. To intuitively observe the phenomenon, IR image was adopted in our experiment to detect the climbing height of cold water (about 10 °C), exhibiting ~8 mm height of the water within 30 min (Figure 3b). In addition, the saturated water absorption of the PP-based samples was also performed in Figure 3c. Compared with the fresh PP (3.03 g/g), the FPP and FPyPP show a remarkable increase of the water absorption of 10.63 g/g and 16.43 g/g, respectively.

Furthermore, to explore the chemical composition of the PP-based samples, energy dispersion spectrum (EDS), X-ray photoelectron spectroscopy (XPS) and Raman spectra were employed in our work. As shown in Figure 3d, Figure S8 and S9, there is more N element on the FPyPP sample than that of FPP. The EDS result illustrates that the PPy polymer is successfully introduced into our system. In addition, XPS characterization was also conducted to explore the refined peaks. There are three main characteristic peaks that appeared

https://dx.doi.org/10.1021/acssuschemeng.0c00681
ACS Sustainable Chem. Eng. 2020, 8, 5328−5337

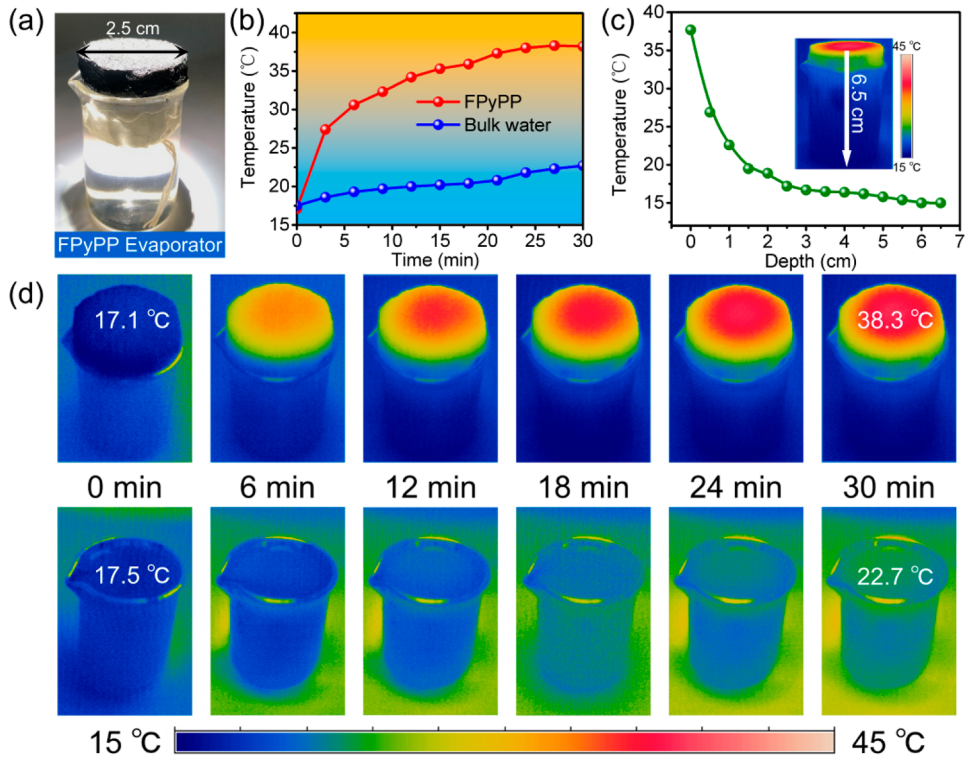

Figure 4. (a) Photograph of FPyPP-based solar evaporator on polystyrene foam under 1 sun irradiation. (b) Surface temperature of FPyPP and bulk water versus time curves. (c) Vertical temperature distribution curve and corresponding 2D IR image of FPyPP. (d) 2D IR images of FPyPP and bulk water under 1 sun irradiation.

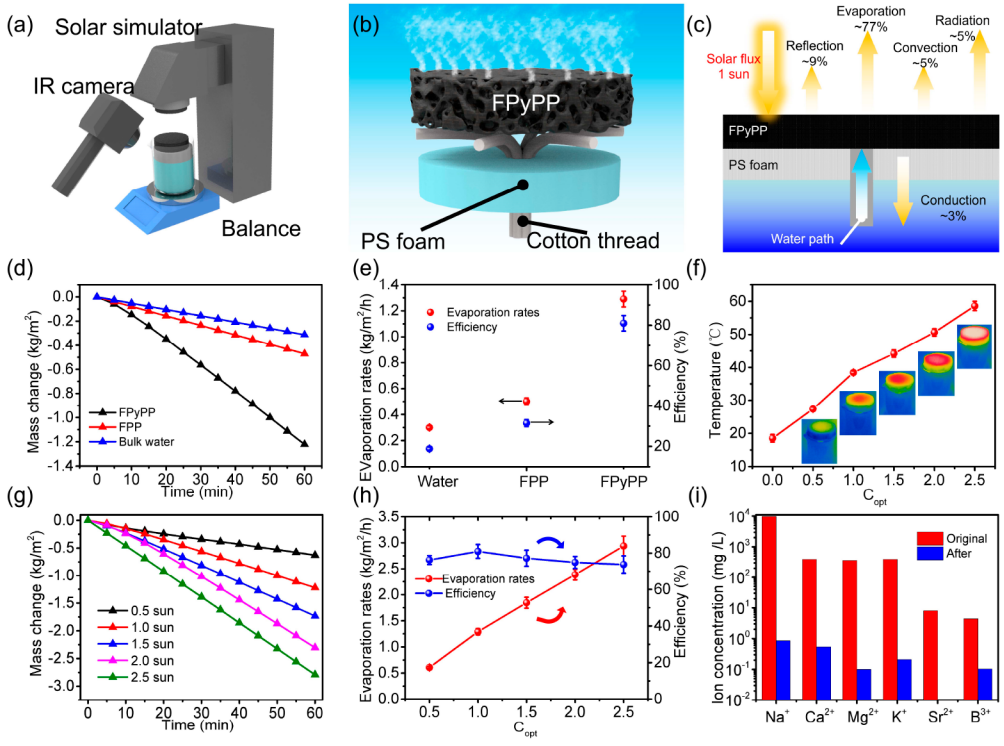

Figure 5. (a) Schematic illustration of simulated solar evaporation experiment. (b) Sketch of the FPyPP-based evaporator. (c) Energy balance and heat loss diagram of FPyPP-based evaporator under 1 sun illumination. (d) Mass change versus time curves of FPyPP, FPP, and bulk water under 1 sun. (e) Evaporation rates and efficiency of FPyPP, FPP, and bulk water under 1 sun. (f) Surface temperature curve and corresponding 2D IR images of FPyPP-based evaporator under different solar intensities. (g) Mass change of FPyPP-based evaporator versus time curves under a series of solar irradiations ranging from 0.5 to 2.5 kW/m^2. (h) Evaporation rates and efficiency curves under different solar intensities. (i) Ion concentration of six simulated seawater samples before and after desalination.

https://dx.doi.org/10.1021/acssuschemeng.0c00681
ACS Sustainable Chem. Eng. 2020, 8, 5328−5337

both in FPP and FPyPP samples at the binding energies of 285 eV, 400 and 532 eV belonging to C 1s, N 1s and O 1s (Figure 3e). Regarding the high-resolution C 1s spectra, the FPP displayed three fitting peaks at 284.2 eV (C−C bonds), 285.9 eV (C−O bonds) and 288.8 eV (C−O) (Figure 3f). For the FPyPP sample, the C 1s spectra exhibited four fitting peaks at 284.4 eV (C−C bonds), 285.6 eV (C−N bonds), 286.1 eV (C = N bonds) and 287.5 eV (C = O bonds) (Figure 3f).[50] Moreover, compared with the peaks of FPP, the Raman spectra clearly illustrate that the FPyPP and PPy samples demonstrate similar characteristic peaks, resulting in successful modification of photothermal PPy polymer on FPP surface (Figure 3g). To further investigate the light absorption performance, an ultraviolet visible-near-infrared (UV−vis-NIR) spectrophotometer was employed. As displayed in Figure S10, compared with the high reflection of FPP, the reflectance of FPyPP demonstrates a remarkable decrease with the value of ∼2% and ∼9% under dry and wet state, respectively. As a result, the average light absorption of the dry and wet FPyPP can reach up to more than 95% over the wavelength range from 400 to 2500 nm(Figure 3h). Owing to the prominent improvement of the light absorption, the solar enery-to-heat conversion performance of the achieved FPyPP can experience favorable enhancement. Superior to the dried FPP with a value of 27.5 °C within 360 s, the dried FPyPP sample can reach up to 54 °C within 360 s under 1 sun irradiation. The result strongly illustrates that the conjugated polypyrrole can significantly enhance the photothermal property for further application (Figure 3i).

In our evaporation system, the polystyrene foam was used to reduce the possible thermal diffusion and the cotton thread was employed to pump water from the bulk water for continuous and stable evaporation (Figure 4a). When the FPyPP was introduced into the evaporator, the surface temperature of FPyPP can reach up to ∼38.3 °C, which is 15.6 °C higher than that of bulk water within 30 min under 1 sun (Figure 4b). Owing to the absorption of water molecules with high specific capacity, the surface temperature of FPyPP can experience a remarkable decrease. However, the relatively low temperature can effectively decrease the thermal irradiation to the environment and still realize a considerable evaporation rate. To investigate the thermal diffusion behavior of the achieved FPyPP-based evaporator, the temperature distribution in the vertical direction was also conducted. It can be clearly observed in Figure 4c that the thermal energy is mainly confined to the surface of the FPyPP. The prominent temperature gradient derives from the polystyrene foam, which can both function as thermal insulator and floating carrier. Specifically, 2D IR images further show the process of surface temperature rise (Figure 4d). There is a remarkable temperature contrast between FPyPP and bulk water under 1 sun illumination, representing the desirable solar-to-thermal conversion of FPyPP.

For the solar-driven interfacial evaporation application, quantitative experiments were conducted to investigate the evaporation performance using a solar simulator-based apparatus (Figure 5a). In our system, a bilayer structure is rationally designed to achieve an effective evaporation with reduced heat loss (Figure 5b). Specifically, the polystyrene foam and cotton thread were used to block the thermal diffusion and to pump water for the FPyPP-based evaporator, respectively. As shown in Figure 5c, the heat loss diagram of FPyPP evaporator in the process of solar steam generation was illustrated, including reflection loss (∼9%), radiation heat loss (∼5%), convection heat loss (∼5%) and conduction heat loss (∼3%), which were calculated according to previous reports.[51−53] The detailed analysis can be found in Supporting Information. In addition, the average thermal conductivities of FPP and FPyPP were also measured, which was 0.707 and 0.293 W/(m·K), respectively. Owing to the introduction of photothermic PPy with low thermal conductivity and bilayer evaporator structure, an effective evaporation system can be established.

It can be found that the FPyPP, FPP and bulk water present the evaporation rates of 1.22 kg/m^2/h, 0.47 kg/m^2/h and 0.31 kg/m^2/h, respectively (Figure 5d). Note that we have also prepared control evaporation experiment of samples with variable pores in the thickness direction, which demonstrates a similar evaporation rate of 1.219 kg/m^2/h (Figure S11). In addition, the evaporation performance of CPP was also investigated in our system. As shown in Figure S12a, the 2D IR characterization was first conducted to explore the solar-to-thermal conversion of CPP, which represented a relatively low temperature of CPP under 1 sun. As a result, the evaporation rate of CPP was about 1.09 kg/m^2/h (Figure S12b). To calculate the photothermal efficiency, the following formula of

$$\eta = mh/I \quad (1)$$

is used for calculating the solar conversion efficiency. In this formula, η is the conversion efficiency; m denotes the mass flux; h is the total enthalpy of the liquid−liquid sensible heat from initial temperature to equilibrium temperature and liquid−vapor latent heat; and I is the input power of solar illumination. The unmodified porous FPP is expected to divide bulk water into numerous small parts, resulting in an improvement of solar energy-to-heat conversion efficiency from 19.57% of bulk water to 29.68%. Furthermore, the introduction of PPy can significantly improve the efficiency, which can reach up to 76.61% under 1 sun (Figure 5e). Since the solar intensity can highly affect the performance of the solar evaporator, the evaporation experiments under a series of solar intensity were conducted. As displayed in Figure 5f, with the increase of solar intensity, the saturated surface temperature of FPyPP represents a gradual increase tendency from 27.9 °C under 0.5 sun to 57.7 °C under 2.5 sun. The achieved evaporation rates also demonstrate a similar increase trend from 0.629 kg/m^2/h to 2.79 kg/m^2/h (Figure 5g). However, higher surface temperature may result in higher heat loss. As a result, the efficiency of FPyPP under 0.5 sun can realize a high value of 79.01%. When the solar intensity was elevated from 0.5 sun to 2.5 sun, the resulted efficiency can experience a decrease process from 79.01% to 69.27% (Figure 5h).

Since the durability is a critical factor for the solar evaporators, the long-term evaporation experiments are conducted in our system. As displayed in Figure S13, the achieved FPyPP was evaluated in the solar desalination test for 96 h constantly. Note that the evaporation rates of FPyPP can experience a fluctuation between 1.28 and 1.4 kg/m^2/h under 1 sun illumination during the whole test process. The result illustrates that the FPyPP evaporator can achieve a stable, continuous and long-term evaporation process. In addition, no obvious salt crystal aggregated was observed on the surface of FPyPP after a desalination of 96 h. The result strongly demonstrates a robust stability of FPyPP in long-time and continuous solar water evaporation. Note that owing to the effective decoration of photothermic PPy on PP surface, the

https://dx.doi.org/10.1021/acssuschemeng.0c00681
ACS Sustainable Chem. Eng. 2020, 8, 5328−5337

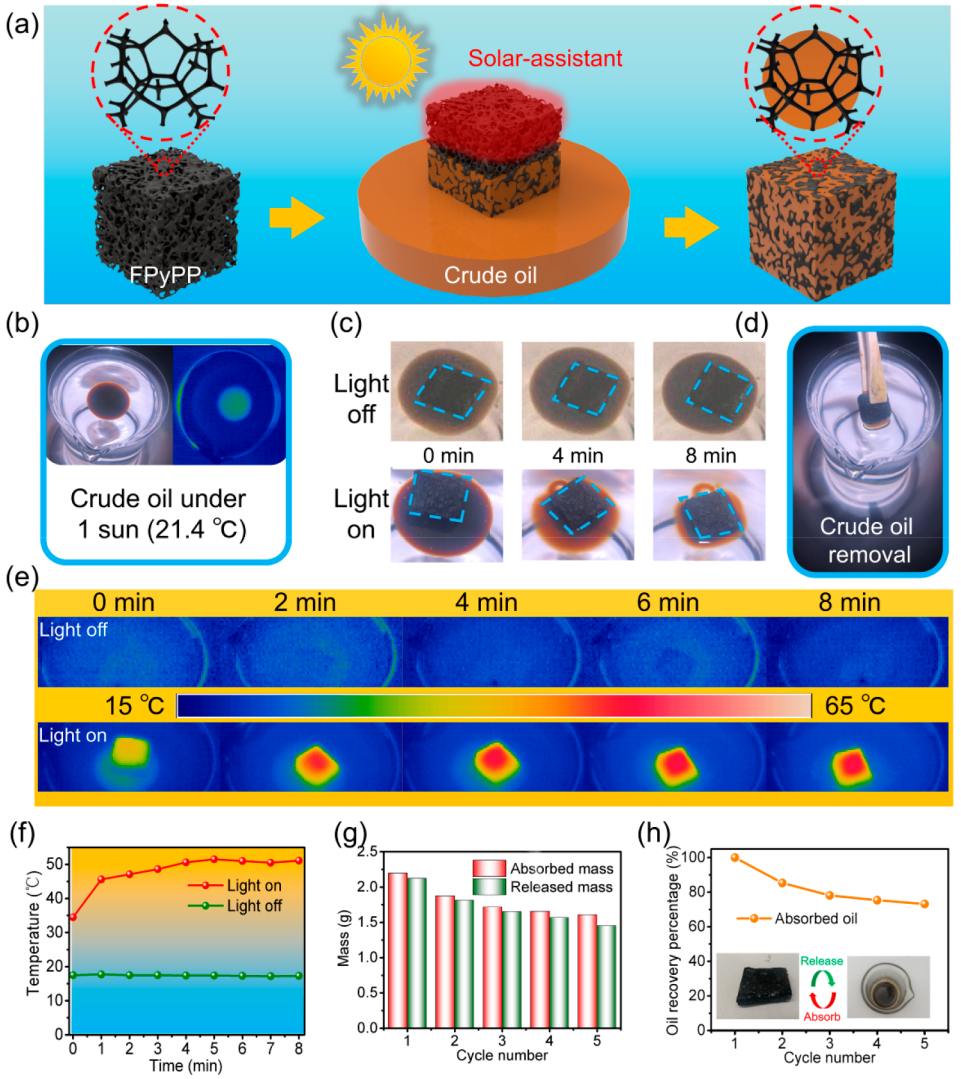

Figure 6. (a) Schematic illustration of the FPyPP-based solar absorber for heavy viscous crude oil removal via solar-assisted heating. (b) Photograph and IR images of crude oil under 1 sun illumination. (c) Photographs of crude oil removal experiments with and without solar irradiation. (d) Photograph of the complete removal of heavy crude oil. (e) IR images of heavy crude oil cleanup by FPyPP with and without solar irradiation within 8 min. (f) Surface temperature versus time curves of FPyPP absorber with and without sun irradiation. (g) Oil absorption–recovery cycles column under 1 sun. (h) Corresponding oil recovery percentage in 5 cycles.

biomass-derived solar evaporators can experience favorable stability. When the FPyPP was floated on the simulated seawater surface under 1 sun irradiation for 12 h per day, the evaporation rate could still maintain about 1.32 kg/m^2/h even after 7 days (Figure S14). The relatively stable evaporation performance can further illustrate that pores inside the FPyPP may not collapse, demonstrating a desirable durability.

Specifically, we also investigated the desalination performance of the FPyPP system. It can be clearly observed that the concentrations of six ions of Na^+, Ca^{2+}, Mg^{2+}, K^+, Sr^{2+} and B^{3+} were prominently reduced in collected clean water, which is lower than that of the World Health Organization (WHO) standard (Figure 5i). In addition, the cycle experiments were also conducted to explore the desalination stability of the FPyPP-based evaporators. For each cycle experiment, the resistance of the achieved purified water was measured for 10 cycles using the multimeter with the distance between two electrodes of about 1.2 cm. The result illustrates that the resistance of purified water in each sample has just a slight fluctuation, demonstrating the favorable capacity of stable desalination (Figure S15).

Benefiting from special coordination effect of amino groups on the polypyrrole, the fabricated FPyPP was chosed to absorb heavy metal ions such as Cr (VI) ions in water while evaporating (Figure S16a).[54] Practically, the sample was placed in a beaker, stirred at a constant speed using a magnetic stirrer, and sampled at a specified time point. Furthermore, to visualize the process of adsorption of Cr (VI), chromogenic reagent was added into the solution samples for color rendering. Notably, compared to the slightly change in color of the resulting solution with FPP, the color of solution treating with FPyPP was absolutely faded, which was derived from the special coordination between amino groups and Cr (VI) (Figures S16b-**d**). Moreover, ultraviolet spectra were also applied to detect the performance of removal of Cr (VI). As shown in Figures S16e and S16f, Cr (VI) (5 mg/L) could be absolutely purified with FPyPP in 150 s, but mostly remained in the resulting solution treated with FPP. Theoretically, the removal capacity was quantitatively calculated. The ultraviolet

https://dx.doi.org/10.1021/acssuschemeng.0c00681
ACS Sustainable Chem. Eng. 2020, 8, 5328−5337

absorption intensity of Cr (VI) solution with concentration of 1−5 mg/L after adding chromogenic agent was first tested. Subsequently, the relationship between absorbance and concentration was obtained via linear fittin as following (Figure S17):

$$A = 0.2186C + 0.0536 \quad (2)$$

where C is the concentration of Cr(VI) and A is the absorbance at 542 nm obtained from the UV test.

The Cr (VI) removal percentage (R%) is calculated:

$$R/\% = \frac{C_0\text{-}C_e}{C_0} \times 100 \quad (3)$$

Where C_0 and C_e (mg/L) are the Cr(VI) concentrations in solution before and after treatment, respectively.

The removal capacity (Q, mg/g) is calculated:

$$Q = \frac{C_0\text{-}C_e}{m} V \quad (4)$$

Where V (L) represents the volume of Cr (VI) solution and m (g) is the mass of the used FPyPP. After calculation, we can conclude that the removal rate is 100%.

Owing to its inner abundant pores, porous materials can effectively absorb organic solvents via capillary force (Figures S18). The FPyPP can absorb Mineral oil 3.2077 g/g, *n*-Heptane 2.5356 g/g, Petroleum ether 2.0667 g/g, and Silicone oil 2.9283 g/g (Figure S19). However, it is challenging for most of porous materials to absorb high-viscosity crude oil, because crude oil will cause blockage of holes due to its low fluidity. Based on the desirable solar-to-thermal conversion property of FPyPP, it can be further employed to *in situ* heat the heavy crude oil. The viscosity of the oil will be remarkably reduced under solar illumination, which can be further absorbed into the porous network of the FPyPP (Figure 6a). As shown in Figure 6b, a drop of viscous crude oil was dropped onto the water surface, followed by 1 sun irradiation for 10 min. It can be found that the surface temperature of crude oil was just elevated from 18 to 21.4 °C, which was futile for viscosity reduction. To investigate the effect of FPyPP on oil absorption, the photothermal FPyPP was added onto the heavy crude oil surface without solar illumination for 8 min, the area of crude oil was still not changed. When the simulated solar with 1 kW/m^2 was applied on the FPyPP, the viscous crude oil could be gradually absorbed into the FPyPP with the increase of irradiation time (Figure 6c). Finally, almost all the heavy crude oil can be removed from the water surface (Figures 6**d and** S20). Further, we also explore the mechanism of the absorption of crude oil. As shown in Figure S21a, the crude oil we used is very sticky at room temperature. It is noted that compared with the FPyPP with absorbed water, the FPyPP on crude oil surface can reach a higher temperature. According to Beggs−Robinson empirical formula:[55]

$$\log(\log)\,\mu\gamma = a_1 + a_2\gamma_{oil} + a_3 \log T \quad (5)$$

where γ_{oil} is oil gravity (unit: °*API*) and a_1, a_2, a_3 are constants. As illustrated in Figure S21b, the viscosity of crude oil gradually decreased as temperature increased from 20 to 70 °C, which resulted in a promotion of the oil absorption capacity of FPyPP. Besides, the oil absorption capacity of FPyPP at different temperatures also was tested quantitatively to demonstrate this special phenomenon (Figure S21c). Additionally, 2D IR images were adopted to demonstrate the change of surface temperature in the heating process. It can be clearly observed in Figure 6e and 6**f** that there is no prominent temperature difference between FPyPP and background before solar irradiation. Once the simulated solar was applied, the surface temperature of FPyPP could quickly rise up to 50.8 °C within 8 min under 1 sun. The results strongly evidenced that photothermal FPyPP can effectively convert the solar energy into considerable heat, resulting in a joule heat assisted viscosity reduction of heavy crude oil. Moreover, the abundant pores inside the FPyPP can further absorb the oil with relatively low viscosity from the water surface. It is noted that the favorable solar-to-thermal performance and abundant pores are both the important factors. To evidence this point, the FPP was also employed to conduct the solar-assisted crude heavy oil removal experiment. As shown in Figure S22, the control experiment showed that no remarkable oil removal was found in the FPP sample under 1 sun irradiation. The phenomenon illustrates that FPP without photothermic PPy decoration cannot efficiently absorb the crude oil.

In addition, the cycle experiments were also conducted in our system. As displayed in Figure 6g and 6**h**, the FPyPP can experience a recycled utilization for crude oil removal. After 5 times cycles, the FPyPP can still maintain a high percentage of oil recovery (over 75%) of oil absorption and release. This photothermal material has provided an alternative pathway to tackle the emergency of heavy crude oil leakage.

CONCLUSIONS

In summary, an environmentally friendly and biocompatible photothermal sponge was fabricated via the rational combination of conjugated PPy polymers and self-templated pomelo peels in a simple and accessible way. Its preparation form is very simple with low-energy-consumption and low-cost. The food waste-based pomelo peels are endowed with abundant capillary pores, which may allow continuous water pumping and/or organics absorption. The PPy-modified photothermal sponge can be employed to achieve solar-driven interfacial water evaporation and further realized solar-heating-enabled heavy crude oil removal. This biomass-derived photothermal sponge can provide a biocompatible platform for realization of seawater purification and heavy crude oil removal without causing secondary pollution or potential negative hazard to the surrounding environment.

ASSOCIATED CONTENT

Supporting Information

The Supporting Information is available free of charge at https://pubs.acs.org/doi/10.1021/acssuschemeng.0c00681.

Photographs, preparing fabrication, pore size distribution, SEM images, EDS mapping images, reflection spectra, evaporation test, ultraviolet adsorption spectra, and absorption test (PDF)

AUTHOR INFORMATION

Corresponding Authors

Wenqin Wang − *School of Materials Science and Chemical Engineering, Ningbo University, Ningbo, Zhejiang 315211, China;* orcid.org/0000-0002-2302-1467; Email: wqwang@126.com

Peng Xiao − *Key Laboratory of Marine Materials and Related Technologies, Zhejiang Key Laboratory of Marine Materials and Protective Technologies, Ningbo Institute of Materials*

https://dx.doi.org/10.1021/acssuschemeng.0c00681
ACS Sustainable Chem. Eng. 2020, 8, 5328−5337

Technology and Engineering, Chinese Academy of Sciences, Ningbo, Zhejiang 315201, China; orcid.org/0000-0003-2231-9824; Email: xiaopeng@nimte.ac.cn

Tao Chen − *Key Laboratory of Marine Materials and Related Technologies, Zhejiang Key Laboratory of Marine Materials and Protective Technologies, Ningbo Institute of Materials Technology and Engineering, Chinese Academy of Sciences, Ningbo, Zhejiang 315201, China;* orcid.org/0000-0001-9704-9545; Email: tao.chen@nimte.ac.cn

Authors

Chang Zhang − *School of Materials Science and Chemical Engineering, Ningbo University, Ningbo, Zhejiang 315211, China; Key Laboratory of Marine Materials and Related Technologies, Zhejiang Key Laboratory of Marine Materials and Protective Technologies, Ningbo Institute of Materials Technology and Engineering, Chinese Academy of Sciences, Ningbo, Zhejiang 315201, China*

Feng Ni − *Key Laboratory of Marine Materials and Related Technologies, Zhejiang Key Laboratory of Marine Materials and Protective Technologies, Ningbo Institute of Materials Technology and Engineering, Chinese Academy of Sciences, Ningbo, Zhejiang 315201, China*

Luke Yan − *Polymer Materials & Engineering Department, School of Materials Science & Engineering, Chang'an University, Xi'an, Shanxi 710064, China*

Qingquan Liu − *Hunan Provincial Key Laboratory of Advanced Materials for New Energy Storage and Conversion, Hunan University of Science and Technology, Xiangtan, Hunan 411201, China*

Dong Zhang − *Department of Chemical, Biomolecular and Corrosion Engineering, The University of Akron, Akron, Ohio 44325, United States*

Jincui Gu − *Key Laboratory of Marine Materials and Related Technologies, Zhejiang Key Laboratory of Marine Materials and Protective Technologies, Ningbo Institute of Materials Technology and Engineering, Chinese Academy of Sciences, Ningbo, Zhejiang 315201, China*

Complete contact information is available at: https://pubs.acs.org/10.1021/acssuschemeng.0c00681

Notes

The authors declare no competing financial interest.

■ ACKNOWLEDGMENTS

We thank the Natural Science Foundation of China (Grant Nos. 51803226 and 51573203), the Key Research Program of Frontier Sciences, Chinese Academy of Sciences (Grant No. QYZDB-SSW-SLH036), the Postdoctoral Innovation Talent Support Program (Grant No. BX20180321), the China Postdoctoral Science Foundation (Grant No. 2018M630695), and the Ningbo Science and Technology Bureau (Grant No. 2018A610108).

■ REFERENCES

(1) Chow, J.; Kopp, R. J.; Portney, P. R. Energy Resources and Global Development. *Science* **2003**, *302* (5650), 1528−1531.

(2) Elimelech, M.; Phillip, W. A. The Future of Seawater Desalination: Energy, Technology, and the Environment. *Science* **2011**, *333* (6043), 712−717.

(3) Lin, C. S. K.; Pfaltzgraff, L. A.; Herrero-Davila, L.; Mubofu, E. B.; Abderrahim, S.; Clark, J. H.; Koutinas, A. A.; Kopsahelis, N.; Stamatelatou, K.; Dickson, F.; Thankappan, S.; Mohamed, Z.; Brocklesby, R.; Luque, R. Food Waste as a Valuable Resource for the Production of Chemicals, Materials and Fuels. Current Situation and Global Perspective. *Energy Environ. Sci.* **2013**, *6* (2), 426−464.

(4) Ermgassen, E. K. H. J. Z.; Balmford, A.; Salemdeeb, R. Reduce, Relegalize, and Recycle Food Waste. *Science* **2016**, *352* (6293), 1526−1526.

(5) Kibler, K. M.; Reinhart, D.; Hawkins, C.; Motlagh, A. M.; Wright, J. Food Waste and The Food-Energy-Water Nexus: A Review of Food Waste Management Alternatives. *Waste Manage.* **2018**, *74*, 52−62.

(6) Pham, T. P. T.; Kaushik, R.; Parshetti, G. K.; Mahmood, R.; Balasubramanian, R. Food Waste-to-Energy Conversion Technologies: Current Status and Future Directions. *Waste Manage.* **2015**, *38*, 399−408.

(7) Burschka, J.; Pellet, N.; Moon, S.-J.; Humphry-Baker, R.; Gao, P.; Nazeeruddin, M. K.; Grätzel, M. Sequential Deposition as a Route to High-Performance Perovskite-Sensitized Solar Cells. *Nature* **2013**, *499* (7458), 316−319.

(8) Bi, C.; Chen, B.; Wei, H.; DeLuca, S.; Huang, J. Efficient Flexible Solar Cell based on Composition-Tailored Hybrid Perovskite. *Adv. Mater.* **2017**, *29* (30), 1605900.

(9) Wang, J.; Chen, H.; Wei, S. H.; Yin, W. J. Materials Design of Solar Cell Absorbers Beyond Perovskites and Conventional Semiconductors via Combining Tetrahedral and Octahedral Coordination. *Adv. Mater.* **2019**, *31* (17), 1806593.

(10) Ren, H.; Tang, M.; Guan, B.; Wang, K.; Yang, J.; Wang, F.; Wang, M.; Shan, J.; Chen, Z.; Wei, D.; Peng, H.; Liu, Z. Hierarchical Graphene Foam for Efficient Omnidirectional Solar-Thermal Energy Conversion. *Adv. Mater.* **2017**, *29* (38), 1702590.

(11) Wang, X.; Liu, Q.; Wu, S.; Xu, B.; Xu, H. Multilayer Polypyrrole Nanosheets with Self-Organized Surface Structures for Flexible and Efficient Solar−Thermal Energy Conversion. *Adv. Mater.* **2019**, *31* (19), 1807716.

(12) Tao, P.; Ni, G.; Song, C.; Shang, W.; Wu, J.; Zhu, J.; Chen, G.; Deng, T. Solar-driven interfacial evaporation. *Nat. Energy* **2018**, *3* (12), 1031−1041.

(13) Li, J.; Du, M.; Lv, G.; Zhou, L.; Li, X.; Bertoluzzi, L.; Liu, C.; Zhu, S.; Zhu, J. Interfacial Solar Steam Generation Enables Fast-Responsive, Energy-Efficient, and Low-Cost Off-Grid Sterilization. *Adv. Mater.* **2018**, *30* (49), 1805159.

(14) Zhang, L.; Tang, B.; Wu, J.; Li, R.; Wang, P. Hydrophobic Light-to-Heat Conversion Membranes with Self-Healing Ability for Interfacial Solar Heating. *Adv. Mater.* **2015**, *27* (33), 4889−4894.

(15) Luo, Y.; Fu, B.; Shen, Q.; Hao, W.; Xu, J.; Min, M.; Liu, Y.; An, S.; Song, C.; Tao, P.; Wu, J.; Shang, W.; Deng, T. Patterned Surfaces for Solar-Driven Interfacial Evaporation. *ACS Appl. Mater. Interfaces* **2019**, *11* (7), 7584−7590.

(16) Zhang, X.; Gao, W.; Su, X.; Wang, F.; Liu, B.; Wang, J.-J.; Liu, H.; Sang, Y. Conversion of Solar Power to Chemical Energy Based on Carbon Nanoparticle Modified Photo-thermoelectric Generator and Electrochemical Water Splitting System. *Nano Energy* **2018**, *48*, 481−488.

(17) Ding, T.; Zhu, L.; Wang, X.-Q.; Chan, K. H.; Lu, X.; Cheng, Y.; Ho, G. W. Hybrid Photothermal Pyroelectric and Thermogalvanic Generator for Multisituation Low Grade Heat Harvesting. *Adv. Energy Mater.* **2018**, *8* (33), 1802397.

(18) Wang, X. Q.; Tan, C. F.; Chan, K. H.; Xu, K.; Hong, M.; Kim, S. W.; Ho, G. W. Nanophotonic-Engineered Photothermal Harnessing for Waste Heat Management and Pyroelectric Generation. *ACS Nano* **2017**, *11* (10), 10568−10574.

(19) Li, K.; Chang, T. H.; Li, Z.; Yang, H.; Fu, F.; Li, T.; Ho, J. S.; Chen, P. Y. Biomimetic MXene Textures with Enhanced Light-to-Heat Conversion for Solar Steam Generation and Wearable Thermal Management. *Adv. Energy Mater.* **2019**, *9* (34), 1901687.

(20) Zhu, Z.; Zhang, J.; Tong, Y. -l.; Peng, G.; Cui, T.; Wang, C.-F.; Chen, S.; Weitz, D. A. Reduced Graphene Oxide Membrane Induced Robust Structural Colors toward Personal Thermal Management. *ACS Photonics* **2019**, *6* (1), 116−122.

(21) Lyu, S.; He, Y.; Yao, Y.; Zhang, M.; Wang, Y. Photothermal Clothing for Thermally Preserving Pipeline Transportation of Crude Oil. *Adv. Funct. Mater.* **2019**, *29* (27), 1900703.
(22) Zhang, P.; Liu, F.; Liao, Q.; Yao, H.; Geng, H.; Cheng, H.; Li, C.; Qu, L. A Microstructured Graphene/Poly(N-isopropylacrylamide) Membrane for Intelligent Solar Water Evaporation. *Angew. Chem., Int. Ed.* **2018**, *57* (50), 16343−16347.
(23) Wang, X.-Q.; Tan, C. F.; Chan, K. H.; Lu, X.; Zhu, L.; Kim, S.-W.; Ho, G. W. In-built Thermo-Mechanical Cooperative Feedback Mechanism for Self-propelled Multimodal Locomotion and Electricity Generation. *Nat. Commun.* **2018**, *9*, 1−10.
(24) Chang, J.; Shi, Y.; Wu, M.; Li, R.; Shi, L.; Jin, Y.; Qing, W.; Tang, C.; Wang, P. Solar-assisted Fast Cleanup of Heavy Oil Spills Using a Photothermal Sponge. *J. Mater. Chem. A* **2018**, *6* (19), 9192−9199.
(25) Kuang, Y.; Chen, C.; Chen, G.; Pei, Y.; Pastel, G.; Jia, C.; Song, J.; Mi, R.; Yang, B.; Das, S.; Hu, L. Bioinspired Solar-Heated Carbon Absorbent for Efficient Cleanup of Highly Viscous Crude Oil. *Adv. Funct. Mater.* **2019**, *29* (16), 1900162.
(26) Zhou, L.; Tan, Y.; Wang, J.; Xu, W.; Yuan, Y.; Cai, W.; Zhu, S.; Zhu, J. 3D Self-assembly of Aluminium Nanoparticles for Plasmon-Enhanced Solar Desalination. *Nat. Photonics* **2016**, *10* (6), 393−398.
(27) Lin, K.; Chen, R.; Zhang, L.; Shen, W.; Zang, D. Enhancing Water Evaporation by Interfacial Silica Nanoparticles. *Adv. Mater. Interfaces* **2019**, *6* (16), 1900369.
(28) Xu, Y.; Ma, J.; Han, Y.; Zhang, J.; Cui, F.; Zhao, Y.; Li, X.; Wang, W. Multifunctional CuO Nanowire Mesh for Highly Efficient Solar Evaporation and Water Purification. *ACS Sustainable Chem. Eng.* **2019**, *7* (5), 5476−5485.
(29) Dudchenko, A. V.; Chen, C.; Cardenas, A.; Rolf, J.; Jassby, D. Frequency-dependent Stability of CNT Joule Heaters in Ionizable Media and Desalination Processes. *Nat. Nanotechnol.* **2017**, *12* (6), 557−564.
(30) Yang, Y.; Zhao, R.; Zhang, T.; Zhao, K.; Xiao, P.; Ma, Y.; Ajayan, P. M.; Shi, G.; Chen, Y. Graphene-Based Standalone Solar Energy Converter for Water Desalination and Purification. *ACS Nano* **2018**, *12* (1), 829−835.
(31) Zhang, P.; Li, J.; Lv, L.; Zhao, Y.; Qu, L. Vertically Aligned Graphene Sheets Membrane for Highly Efficient Solar Thermal Generation of Clean Water. *ACS Nano* **2017**, *11* (5), 5087−5093.
(32) Xiao, P.; Gu, J.; Zhang, C.; Ni, F.; Liang, Y.; He, J.; Zhang, L.; Ouyang, J.; Kuo, S.-W.; Chen, T. A Scalable, Low-cost and Robust Photo-thermal Fabric with Tunable and Programmable 2D/3D Structures Towards Environmentally Adaptable Liquid/solid-medium Water Extraction. *Nano Energy* **2019**, *65*, 104002.
(33) Ghasemi, H.; Ni, G.; Marconnet, A. M.; Loomis, J.; Yerci, S.; Miljkovic, N.; Chen, G. Solar Steam Generation by Heat Localization. *Nat. Commun.* **2014**, *5*, 4449.
(34) Zhou, X.; Zhao, F.; Guo, Y.; Zhang, Y.; Yu, G. A Hydrogel-based Antifouling Solar Evaporator for Highly Efficient Water Desalination. *Energy Environ. Sci.* **2018**, *11* (8), 1985−1992.
(35) Zeng, J.; Wang, Q.; Shi, Y.; Liu, P.; Chen, R. Osmotic Pumping and Salt Rejection by Polyelectrolyte Hydrogel for Continuous Solar Desalination. *Adv. Energy Mater.* **2019**, *9* (38), 1900552.
(36) Zhao, F.; Zhou, X.; Shi, Y.; Qian, X.; Alexander, M.; Zhao, X.; Mendez, S.; Yang, R.; Qu, L.; Yu, G. Highly Efficient Solar Vapour Generation via Hierarchically Nanostructured Gels. *Nat. Nanotechnol.* **2018**, *13* (6), 489−495.
(37) Singh, S.; Shauloff, N.; Jelinek, R. Solar-Enabled Water Remediation via Recyclable Carbon Dot/Hydrogel Composites. *ACS Sustainable Chem. Eng.* **2019**, *7* (15), 13186−13194.
(38) Zhu, L.; Ding, T.; Gao, M.; Peh, C. K. N.; Ho, G. W. Shape Conformal and Thermal Insulative Organic Solar Absorber Sponge for Photothermal Water Evaporation and Thermoelectric Power Generation. *Adv. Energy Mater.* **2019**, *9* (22), 1900250.
(39) Zhang, Y.; Yin, X.; Yu, B.; Wang, X.; Guo, Q.; Yang, J. Recyclable Polydopamine-Functionalized Sponge for High-Efficiency Clean Water Generation with Dual-Purpose Solar Evaporation and Contaminant Adsorption. *ACS Appl. Mater. Interfaces* **2019**, *11* (35), 32559−32568.
(40) Zhang, Z.; Mu, P.; He, J.; Zhu, Z.; Sun, H.; Wei, H.; Liang, W.; Li, A. Facile and Scalable Fabrication of Surface-Modified Sponge for Efficient Solar Steam Generation. *ChemSusChem* **2019**, *12* (2), 426−433.
(41) Gong, F.; Li, H.; Wang, W.; Huang, J.; Xia, D.; Liao, J.; Wu, M.; Papavassiliou, D. V. Scalable, Eco-friendly and Ultrafast Solar Steam Generators Based on One-step Melamine-derived Carbon Sponges Toward Water Purification. *Nano Energy* **2019**, *58*, 322−330.
(42) Liu, H.; Chen, C.; Chen, G.; Kuang, Y.; Zhao, X.; Song, J.; Jia, C.; Xu, X.; Hitz, E.; Xie, H.; Wang, S.; Jiang, F.; Li, T.; Li, Y.; Gong, A.; Yang, R.; Das, S.; Hu, L. High-Performance Solar Steam Device with Layered Channels: Artificial Tree with a Reversed Design. *Adv. Energy Mater.* **2018**, *8* (8), 1701616.
(43) Xu, N.; Hu, X.; Xu, W.; Li, X.; Zhou, L.; Zhu, S.; Zhu, J. Mushrooms as Efficient Solar Steam-Generation Devices. *Adv. Mater.* **2017**, *29* (28), 1606762.
(44) Fang, J.; Liu, J.; Gu, J.; Liu, Q.; Zhang, W.; Su, H.; Zhang, D. Hierarchical Porous Carbonized Lotus Seedpods for Highly Efficient Solar Steam Generation. *Chem. Mater.* **2018**, *30* (18), 6217−6221.
(45) Li, Z.; Wang, C.; Lei, T.; Ma, H.; Su, J.; Ling, S.; Wang, W. Arched Bamboo Charcoal as Interfacial Solar Steam Generation Integrative Device with Enhanced Water Purification Capacity. *Adv. Sustain. Systems* **2019**, *3* (4), 1800144.
(46) Long, Y.; Huang, S.; Yi, H.; Chen, J.; Wu, J.; Liao, Q.; Liang, H.; Cui, H.; Ruan, S.; Zeng, Y.-J. Carrot-inspired solar thermal evaporator. *J. Mater. Chem. A* **2019**, *7* (47), 26911−26916.
(47) Wang, Y.; Wang, C.; Song, X.; Huang, M.; Megarajan, S. K.; Shaukat, S. F.; Jiang, H. Improved Light-harvesting and Thermal Management for Efficient Solar-driven Water Evaporation Using 3D Photothermal Cones. *J. Mater. Chem. A* **2018**, *6* (21), 9874−9881.
(48) Ni, F.; Xiao, P.; Qiu, N.; Zhang, C.; Liang, Y.; Gu, J.; Xia, J.; Zeng, Z.; Wang, L.; Xue, Q.; Chen, T. Collective Behaviors Mediated Multifunctional Black Sand Aggregate Towards Environmentally Adaptive Solar-to-thermal Purified Water Harvesting. *Nano Energy* **2020**, *68*, 104311.
(49) Mu, P.; Bai, W.; Fan, Y.; Zhang, Z.; Sun, H.; Zhu, Z.; Liang, W.; Li, A. Conductive Hollow Kapok Fiber-PPy Monolithic Aerogels With Excellent Mechanical Robustness for Efficient Solar Steam Generation. *J. Mater. Chem. A* **2019**, *7* (16), 9673−9679.
(50) Liang, Q.; Ye, L.; Huang, Z. H.; Xu, Q.; Bai, Y.; Kang, F.; Yang, Q. H. A Honeycomb-like Porous Carbon Derived from Pomelo Peel for Use in High-performance Supercapacitors. *Nanoscale* **2014**, *6* (22), 13831−13837.
(51) Ni, G.; Li, G.; Boriskina, S. V.; Li, H.; Yang, W.; Zhang, T.; Chen, G. Steam Generation under One Sun Enabled by a Floating Structure with Thermal Concentration. *Nat. Energy* **2016**, *1*, 1−7.
(52) Zhang, P.; Liao, Q.; Zhang, T.; Cheng, H.; Huang, Y.; Yang, C.; Li, C.; Jiang, L.; Qu, L. High Throughput of Clean Water Excluding Ions, Organic Media, and Bacteria from Defect-abundant Graphene Aerogel under Sunlight. *Nano Energy* **2020**, *70*, 104557.
(53) Ni, G.; Zandavi, S. H.; Javid, S. M.; Boriskina, S. V.; Cooper, T. A.; Chen, G. A Salt-rejecting Floating Solar Still for Low-cost Desalination. *Energy Environ. Sci.* **2018**, *11* (6), 1510−1519.
(54) Muhammad Ekramul Mahmud, H. N.; Huq, A. K. O.; Yahya, R. b. The Removal of Heavy Metal Ions from Wastewater/Aqueous Solution Using Polypyrrole-Based Adsorbents: A Review. *RSC Adv.* **2016**, *6* (18), 14778−14791.
(55) Egbogah, E. O.; Ng, J. T. An Improved Temperature-Viscosity Correlation for Crude Oil Systems. *J. Pet. Sci. Eng.* **1990**, *4* (3), 197−200.

https://dx.doi.org/10.1021/acssuschemeng.0c00681
ACS Sustainable Chem. Eng. 2020, 8, 5328−5337